Ocean Engineering 137 (2017) 394–403

Contents lists available at ScienceDirect

Ocean Engineering

journal homepage: www.elsevier.com/locate/oceaneng

The power-capture of a nearshore, modular, flap-type wave energy converter in regular waves

L. Wilkinson[a,b,*], T.J.T. Whittaker[b], P.R. Thies[c], A. Day[d], D. Ingram[e]

[a] Industrial Doctoral Centre for Offshore Renewable Energy (IDCORE), United Kingdom
[b] Marine Research Group, School of Natural and Built Environment, David Keir Building, Stranmillis Road, Queen's University Belfast, Belfast BT9 5AG, United Kingdom
[c] College of Engineering, Mathematics and Physical Sciences, University of Exeter, Penryn Campus, Penryn, Cornwall TR10 9FE, United Kingdom
[d] Naval Architecture and Marine Engineering, University of Strathclyde, Henry Dyer Building, 100 Montrose St, Glasgow G4 0LZ, United Kingdom
[e] Institute for Energy Systems, The University of Edinburgh, Faraday Building, King's Buildings, Colin Maclaurin Road, Edinburgh EH9 3DW, United Kingdom

ARTICLE INFO

Keywords:
Wave energy converter
Power
Modular Flap

ABSTRACT

Bottom-hinged, nearshore flap-type wave energy converters (WECs), have several advantages, such as high power conversion efficiency and survivability. They typically comprise a single flap spanning their full width. However, a potentially beneficial design change would be to split the flap into multiple modules, to make a 'Modular Flap'. This could provide improvements, such as increased power-capture, reduced foundation loads and lower manufacturing and installation costs. Assessed in this work is the hydrodynamic power-capture of this device, based on physical modelling. Comparisons are made to an equivalent 'Rigid Flap'. Tests are conducted in regular, head-on and off-angle waves. The simplest control strategy, of damping each module equally, is employed.

The results show that, for head-on waves, the power increases towards the centre of the device, with the central modules generating 68% of the total power. Phase differences are also present. Consequently, the total power produced by the Modular Flap is, on average, 23% more smooth than that generated by the Rigid Flap.

The Modular Flap has 3% and 1% lower average power-capture than the Rigid Flap in head-on and off-angle waves, respectively. The advantages of the modular concept may therefore be exploited without significantly compromising the power-capture of the flap-type WEC.

1. Introduction

There is a need to improve the economic viability of wave energy converters (WECs), for them to compete in the energy market. Design solutions must be found that have high energy yields, whilst offering manageable manufacturing, installation, maintenance and decommissioning costs.

Bottom-hinged flap-type WECs, also known as Oscillating Wave Surge Converters, are designed to absorb energy from the horizontal acceleration of water in ocean waves (Whittaker and Folley, 2012). They usually consist of a buoyant flap, with its hinge mounted on the seabed (Folley et al., 2007). These devices are typically sited in the nearshore region, in water depths of 10–20 m. There is an extensive body of work on this type of device (Henry, 2008; Renzi et al., 2014; van't Hoff, 2009). Through comparative assessments, it has been shown to be one of the most efficient in terms of power conversion (Babarit, 2015; Babarit et al., 2012). It also has cost reduction advantages, such as being located in the relatively accessible nearshore region, being simple in operation and having high survivability (Henry et al., 2010). As a result, the device type has received significant commercial focus, with a number of large scale devices deployed, such as Aquamarine Power Ltd's Oyster machines (Henry et al., 2010; Whittaker and Folley, 2012) and AW-Energy's WaveRoller devices (AW-Energy, 2012).

Most flap-type devices employ a single body for their rotating section (Folley et al., 2007). If this is large, for example 26 m in width like the Oyster 800 device (Aquamarine Power Ltd, 2011), then asymmetric pressure across the flap results in twisting of the structure, including its foundation (Wilkinson et al., 2014). The use of a single wide unit like this can also necessitate the use of large, expensive

* Corresponding author at: Industrial Doctoral Centre for Offshore Renewable Energy (IDCORE), United Kingdom.
E-mail addresses: l.wilkinson@ed.ac.uk (L. Wilkinson), t.whittaker@qub.ac.uk (T.J.T. Whittaker), p.r.thies@exeter.ac.uk (P.R. Thies), sandy.day@strath.ac.uk (S. Day), david.ingram@ed.ac.uk (D. Ingram).

http://dx.doi.org/10.1016/j.oceaneng.2017.04.016
Received 7 January 2017; Received in revised form 12 April 2017; Accepted 14 April 2017
Available online 21 April 2017

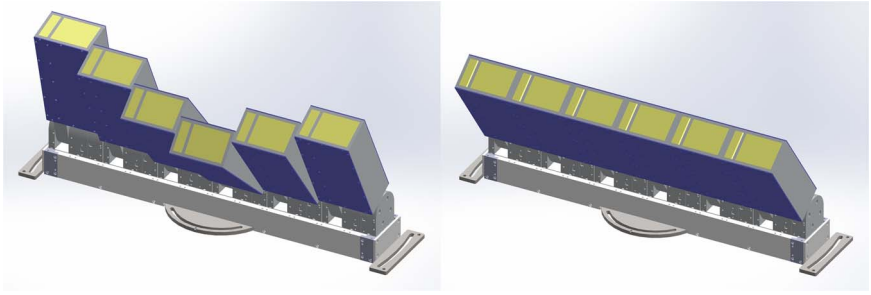

Fig. 1. CAD renderings of physical model in Modular Flap (left) and Rigid Flap (right) configurations.

installation vessels (Aquamarine Power Ltd, 2009). Additionally, the power produced by the device is sensitive to the direction of the incident wave (Henry, 2008). A new concept, the 'Modular Flap', formed by splitting the rotating body into a number of narrow, mechanically independent, vertical modules, may reduce the magnitudes of these problems. This could provide improvements, such as increased power production in directional waves, reduced foundation loads, an indicator of capital cost, and lower manufacturing and installation costs. There could also be operational advantages such as increased redundancy in the system, reducing the effect of failure on one module versus a whole flap. Additionally, a modular formation would make the scaling up of devices, in terms of overall width, arguably more feasible.

There are a number of studies on offshore structures comprised of multiple flaps (Mei et al., 1994; Wilkinson et al., 2014). In Wilkinson et al. (2014), it was shown that the foundation loads were reduced for such a device, by up to 73% in the parasitic twisting yaw and roll degrees of freedom. However, the application of such a device for the purpose of wave energy extraction has only recently received attention (Abadie and Dias, 2016; Álvarez, 2015; Sammarco et al., 2013; Sarkar et al., 2016; Wilkinson et al., 2015). These studies investigated the behaviour of the device, in terms of motion amplitudes, and most of them included a power-capture assessment. The latter is a key element of a techno-economic evaluation of a WEC concept. Sarkar et al. (2016), for example, presents a mathematical power-capture assessment of a 24 m wide device, made up of six cylindrical modules. Regular, head-on waves were used in the study. It was found that the power-capture of the modular system was highly dependent on the power take-off (PTO) damping strategy. With each module damped equally, both devices achieved similar levels of power-capture. However, using different damping on each module, the modular flap outperformed the rigid flap, due to the occurrence of multiple resonances. While this study provided an insight into the potential of the device, there were limitations of the modelling that was used, such as not considering nonlinear and viscous effects (Sarkar et al., 2016). The use of scale physical modelling can address these issues by working in a real fluid. It also provides reasonably fast generation of sufficiently long data time-series, compared to, for example computational fluid dynamics (Abadie and Dias, 2016). In this paper, physical modelling in a wave tank is used to assess the hydrodynamic power-capture of the Modular Flap. This is carried out across a range of wave conditions. Comparisons are made to a single device with an equivalent total width, referred to throughout this work as the 'Rigid Flap'. Shown first, in Section 2, are the modelling and analysis methodologies, followed by presentation of the results in Section 3 and finally, in Section 4, some conclusions and suggestions for further work.

2. Methodology

This section presents the key information on the physical modelling methodology. This includes details on the physical model, the wave conditions, the wave tank and the modelling and analysis procedures that were used. The physical modelling was conducted at 30th scale. Froude scaling was used to convert the variables and results into full-scale values.

2.1. Physical model

The physical model was made up of six box-shaped, surface-piercing modules. The total width of the model was approximately 33 m at full scale, which is similar to the Oyster 800 machine (Aquamarine Power Ltd, 2011). The model could be configured either as the Modular Flap or the Rigid Flap. The Rigid Flap was formed by attaching the modules together with PVC sheets on the front and back faces. The modules, when independent, also had PVC sheets attached to them, to maintain consistent mass and geometric properties. The flap modules were mounted on a base structure, attached to the wave tank floor. 3D CAD renderings of the Modular and Rigid Flaps are provided in Fig. 1; the key dimensions of the model are shown in Fig. 2; the model, installed and operating in the wave tank, is shown in Fig. 3; a diagram illustrating the module numbering system that is used for results presentation is shown in Fig. 4.

At the hinge axis of each module were housings for bearings and instrumentation. The instrumentation included sensors to measure instantaneous rotation and applied damping torque. Each module also contained a magnetic particle brake (MPB), to simulate a Coulomb-

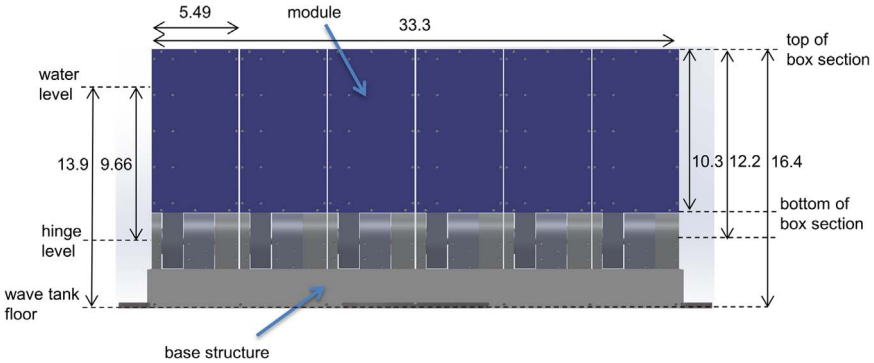

Fig. 2. Device dimensions, in full scale, in m. Note that the thickness of the device was 3.6 m.

Fig. 3. Photograph of the physical model, in its Modular Flap configuration, operating in the wave tank.

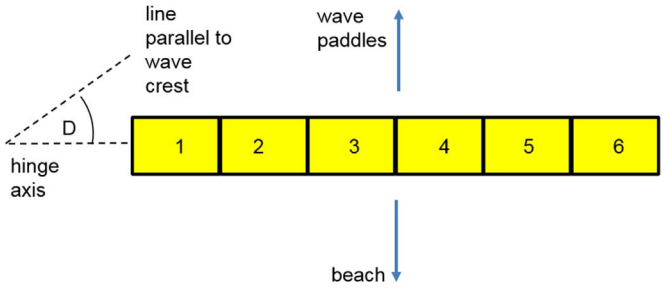

Fig. 4. Plan-view diagram illustrating module numbering and wave direction angle, *D*, reference system. Geometry is to scale.

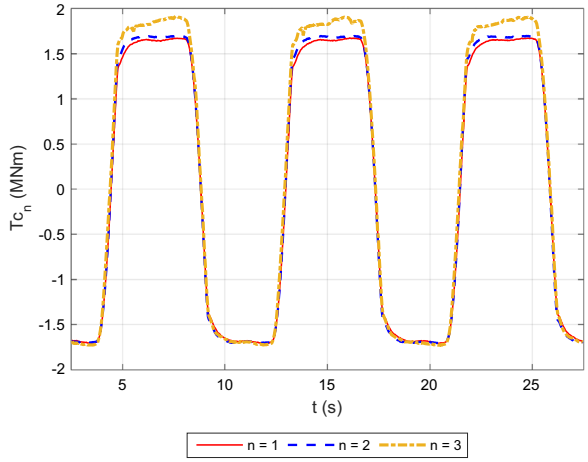

Fig. 5. Example of variation in damping torque, Tc_n, with time, *t*, for the *n*th modules, fixed together in the Rigid Flap configuration.

damping PTO mechanism. Further model details can be found in (Wilkinson et al., 2015). In this study, the simplest control strategy, of applying damping equally to each module, was applied. This was executed by controlling the supply voltages in a LabVIEW program using damping-voltage conversion equations (National Instruments, 2016). The equations were defined by recording the root-mean-square (RMS) damping levels, calculated using Eq. (3), defined later, at different voltage levels and fitting curves to the results. The MPBs had slightly different damping sensitivities to changes in voltage. This was accounted for, though, by using a different damping-voltage conversion equation for each MPB. To illustrate the resulting high level of control that was achieved, example time-series of damping torques for the modules on one side of the Rigid Flap are shown in Fig. 5.

Fig. 5 shows that there were relatively small differences in the applied damping torque for each MPB, notably in the positive direction. These were present partly because the damping was not controlled dynamically and was not completely constant. The RMS damping torques were acceptably close though, with typical variation between the modules within the Rigid Flap only 2%. The consistency and repeatability was sufficiently high too. Hence, the damping system was adequate for use in the study.

2.2. Wave conditions

Regular, head-on waves were used, to generate a fundamental understanding of the Modular Flap. The response of a WEC is generally dependent on the wave period, even for a fairly broad-banded device like a flap-type WEC (Clabby et al., 2012; Whittaker and Folley, 2012). Therefore, one of the chosen variables for this investigation was the wave period. Eight wave periods were used, approximately evenly spaced between 5.5 s and 13.5 s at full scale. These limits represent the typical range for peak periods at a wave energy site (Babarit et al., 2012). Variation in wave amplitude was not considered as it was not thought to be the most significant parameter relating to power capture. A nominal wave amplitude, of 1 m, at full scale, was selected, with maximum variation of only 2%.

The power-capture of a flap-type WEC is sensitive to direction (Henry, 2008). It is hence desirable to mitigate the detrimental effects of increasing wave direction. It is likely that, due to the independence of the modules, the Modular Flap would provide such a solution. Hence, for a small test subset, the wave direction was varied too. Note that for the following sections, the terms ‘head-on’ and ‘off-angle’ are used for cases where the wave direction is 0 and non-0 degrees, respectively. The full range of wave conditions are presented in Table 1.

2.3. Wave tank

The Queen’s University Belfast (QUB) Portaferry Wave Tank (QUB, 2016) was selected for testing due to its suitability for shallow water studies, high wave homogeneity (O’Boyle, 2013) and low blockage ratio. A layout of the wave tank, with the model position indicated, is provided in Fig. 6.

2.4. Modelling and analysis procedures

The aim of the study, as discussed, was to determine the hydrodynamic power-capture achieved by the two devices for a range of wave conditions. To achieve this, the total average powers were recorded for a range of damping levels, for each wave condition. The maximum average powers were then determined by fitting a curve through the damping-power pairs, with the peak providing the maximum power. The power-capture was then evaluated using the metric, capture factor. The mean difference in the capture factor values achieved by the two devices, relative to those associated with the Rigid Flap, was then the

Table 1
List of measured wave conditions that were used.

Wave Identifier	Wave Amplitude, a (m)	Wave Period, T (s)	Incident Wave Power, P_{inc} (kW/m)	Wave Direction, D (deg)
1	0.99	13.5	48.4	0
2	0.99	12.5	46.5	0
3	1.00	10.6	44.6	0
4	0.98	9.5	40.3	0
5	1.01	8.5	39.3	0
6	1.00	7.5	34.6	0
7	1.00	6.5	29.3	0
8	1.00	5.5	23.3	0
9	1.01	8.6	39.5	7.5
10	0.99	8.6	36.2	17.5
11	1.00	8.6	34.1	27.5

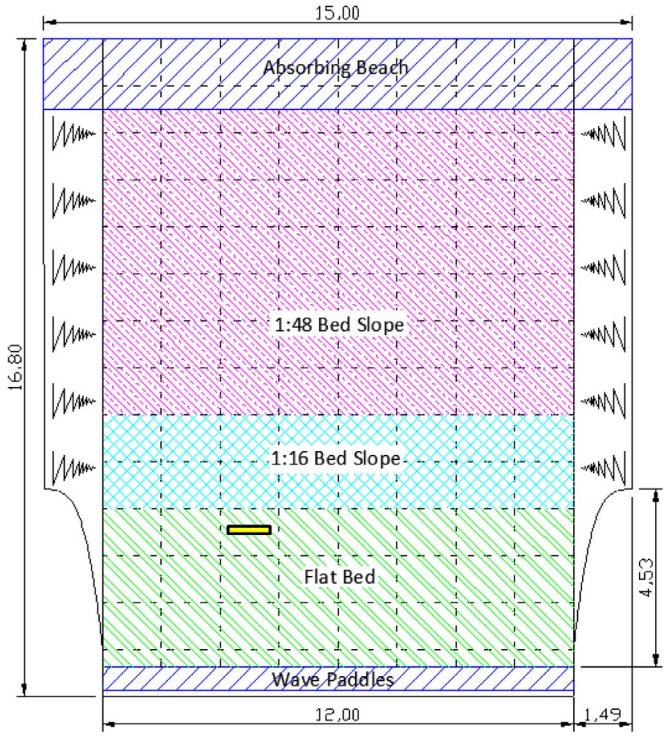

Fig. 6. Portaferry Wave Tank layout, to scale, with model scale dimensions in m (O'Boyle, 2013). Model position is indicated by yellow rectangle. Model geometry is approximately to scale.

ultimate metric that was computed. This analysis process started with evaluation of the instantaneous results and is summarised here.

The two instantaneous measurements that were made were damping torque, Tc_n, in MNm, and rotation, θ_n, in radians (rad.). Data were recorded at 128 Hz, at model scale. θ_n was differentiated with respect to time, to find the angular velocity, $\dot{\theta}_n$, in rad/s. These signals were post-processed using a low-pass filter (MathWorks, 2016), with a cut-off frequency of up to 10 Hz, at model scale. The instantaneous power, P_n, in kW, was then calculated using Eq. (1).

$$P_n = Tc_n \dot{\theta}_n \tag{1}$$

The instantaneous total power, P_T, was then calculated using Eq. (2).

$$P_T = \sum_{n=1}^{M} P_n \tag{2}$$

where M is the number of modules, six.

Each damping level was applied for a duration of 351 s at full scale. The magnitude of each damping level was evaluated as the root-mean-square (RMS) damping torque, $Tc_{n,RMS}$; the equivalent value for the power-capture was the mean power, $\overline{P}_n$. These statistics were generated using Eqs. (3) and (4), respectively.

$$Tc_{n,RMS} = \sqrt{\frac{\sum_{i=1}^{N} Tc_{n,i}{}^2}{N}} \tag{3}$$

$$\overline{P}_n = \frac{\sum_{i=1}^{N} P_{n,i}}{N} \tag{4}$$

where N is the number of samples in the time series.

The device statistics were the total RMS damping torque, $Tc_{RMS,T}$, and total mean power, $\overline{P}_T$, which were calculated using Eqs. (5) and (6), respectively.

$$Tc_{RMS,T} = \sum_{n=1}^{M} Tc_{n,RMS} \tag{5}$$

$$\overline{P}_T = \sum_{n=1}^{M} \overline{P}_n \tag{6}$$

Another point of interest was how smooth the generated power was. A smoother delivery of power to the electrical grid reduces the requirements for energy storage and hence cost (Molinas et al., 2007). The metric for 'smoothness', S_P, was calculated using Eq. (7). Note that a higher S_P value indicates a greater level of smoothing.

$$S_P = \frac{\overline{P}_T}{\sigma_T} \tag{7}$$

Where σ_T is the standard deviation of the instantaneous total power, P_T, defined in Eq. (8).

$$\sigma_T = \sqrt{\frac{1}{N-1} \sum_{i=1}^{N} |P_i - \overline{P}_T|^2} \tag{8}$$

The maximum mean power for each wave condition, for each device, $\overline{P}_{T,max}$, was estimated by fitting a quadratic curve to the $Tc_{RMS,T}$, $\overline{P}_T$ pairs and finding the peak. The x-axis value of this peak corresponded to the optimum damping level. An example power curve is provided in Fig. 7.

The capture factor, CF, is a useful measure of the efficiency of a device (Folley et al., 2007). CF is the ratio of generated power, in this case $\overline{P}_{T,max}$, to incident power and was calculated using Eq. (9).

$$CF = \frac{\overline{P}_T}{P_{inc} \cos(D) W} \tag{9}$$

where, P_{inc} is the incident power per metre of crest, in kW/m; D is the wave direction angle, in rad.; W is the device width, 33.3, in m. P_{inc} was calculated for each wave condition, using standard formulae (United States Naval Academy, n.d.), with the results presented in Table 1.

The relative differences in the CF values achieved by the two devices, using the Rigid Flap as the reference point, $\Delta CF'$, were then computed using Eq. (10).

$$\Delta CF' = \frac{CF_{Mod} - CF_{Rig}}{CF_{Rig}} \tag{10}$$

where CF_{Mod} and CF_{Rig} are the CF values achieved by the Modular and Rigid Flaps, respectively.

The mean relative difference in the CF values, $\overline{\Delta CF'}$, was then computed using Eq. (11).

$$\overline{\Delta CF'} = \frac{\sum_{j=1}^{P} \Delta CF_j{}'}{P} \tag{11}$$

where, for the jth wave condition, $\Delta CF_j{}'$ is the relative difference in CF values and P is the number of wave conditions, for example 8 for the head-on waves.

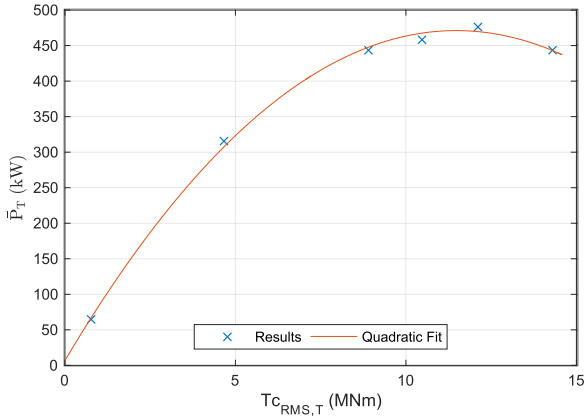

Fig. 7. Example of power curve, showing total mean power, $\overline{P}_T$, against total RMS damping torque, $Tc_{RMS,T}$, with quadratic curve fit.

2.5. Uncertainty analysis

An uncertainty analysis was completed to ascertain the usability of the results for statistical significance of the conclusions that were drawn. This section contains some background information, discussion of the uncertainty sources and a description of the calculation method for the dominant source.

Uncertainties arise from random or systematic errors (Coleman and Steele, 2009), for example due to temperature variation or calibration of sensors, respectively. The outcome of an uncertainty analysis is an estimation of a range, +/- U_X, around the best measurement of a result, X_{best}. It is believed that the true value, X_{true}, lies within this range, to a certain degree of confidence (Coleman and Steele, 2009; Lamont-Kane et al., 2013). In this study, the 95% confidence limit was used, which is standard for engineering applications (Coleman and Steele, 2009; ITTC, 2014). The aim of the uncertainty analysis in this paper was to estimate U_X for the mean relative differences in *CF* between the two devices, $\overline{\Delta CF}$, as defined in Eq. (10), $U_{\overline{\Delta CF}}$.

The uncertainties in the measured variables were propagated to the results through the use of the Taylor Series Method (TSM), a standard technique (Coleman and Steele, 2009). Both random and systematic uncertainties were considered. Only those sources of uncertainty which were deemed significant were accounted for. These are listed below, with the category of the source provided in brackets:

1. Torque sensor calibration slopes (systematic)
2. Rotation sensor calibration accuracy (systematic)
3. Variation of wave conditions and model behaviour (random)
4. Model orientation (systematic)

The dominant source of uncertainties was number 2, the 'rotation sensor calibration accuracy'. These uncertainties were made apparent when the modules were fixed together as the Rigid Flap. The measurements of rotation and angular velocity should have been the same for this configuration. However, it was noticed that there were appreciable differences. This issue was thought to have arisen due to the way in which the sensors were calibrated. The sensors were calibrated simultaneously by first fixing the modules together with an aluminium bar on the front and back faces. For practical reasons, this was conducted outside of the wave tank. The bars were then removed and the modules installed in the wave tank and fixed together with PVC sheets to form the Rigid Flap. The deviations in velocity may have therefore resulted from the slight differences in constraint, between that supplied by the bars and the PVC sheets. A typical example of the velocity differences is shown in Fig. 8. The results presented are for the sensors that displayed the largest differences when compared to the mean results, which are also provided.

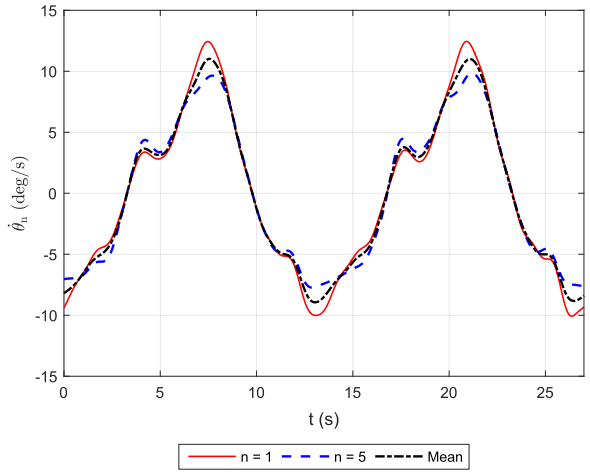

Fig. 8. Example of variation in angular velocity, $\dot{\theta}_n$, with time, *t*, for the *n*th modules, and mean values for all modules. Note that the modules were fixed together in the Rigid Flap configuration.

Fig. 8 shows that the sensors, when compared to the mean results, under or overestimated the magnitudes of the velocities. These deviations resulted in fairly consistent relative percentage differences in the mean absolute angular velocities, between −8 and +7% and, on average, 4%. These disparities were greater than any differences in the applied damping torques and the relative uncertainties associated with these. Hence, it is very likely that the dominant contributions to the velocity differences were rotation sensor uncertainties. As the velocity differences were consistent, they were used to estimate the *systematic* uncertainties on the velocity measurements. For the Rigid Flap, direct comparison to the instantaneous mean of the module velocities was used to calculate these. For the Modular Flap though, as a result of the hydrodynamics, there were natural differences in the velocities of the modules. This meant that a different method had to be applied, which was to use the aforementioned mean relative differences in velocities for each module.

The other sources of uncertainty were significantly smaller than that attributed to the angular velocity measurements, with relative magnitudes of less than 1%. Hence, as mentioned, the dominant source was the angular velocity measurements. Nevertheless, the device power uncertainties were reasonable. As a result, the experimental system was still able to show statistically significant differences in the capture factors achieved by the two devices at certain wave conditions.

3. Results

This section presents the key results from the study. First shown are results for the individual modules with the model configured as the Modular Flap, in Section 3.1, followed by those for the whole devices, in Section 3.2. Within each of these, compared first are the power time-series. Inspection of these allows one to gauge their relative magnitudes and phases. This is followed by presentation of the mean power results. The focus of the section is the head-on wave results because they are the conditions that a flap-type device should be first tested in. Results for the off-angle waves are provided only in the device section.

3.1. Modular Flap modules

Fig. 9 shows an example of power time-series for modules 1–3, which occupied one side of the model. Also shown are time-series of damping torques and velocities, to allow further understanding of the results.

Firstly, subplot c) of Fig. 9 shows that there was a short period of each oscillation where the power was negative. This is thought to have resulted from a spring effect in the dampers when the modules changed direction. This will have injected some torque into the system. For this short period, the damper acted like a motor. The negative power values were included in the calculation of mean power. It is likely though that the effect on the mean power values will have been small. This is because the effect of the negative power phase will likely have been cancelled out by an increase in the positive power due to an increased velocity.

There were also double-peaks present in the velocity and power signals. This may have been due to waves radiated by each flap module interacting with adjacent units. The difference in magnitudes in the maximum values of power for alternate strokes, especially prominent for module 3, were likely due to asymmetry in the surge forces.

The key features of Fig. 9 though are the differences in magnitudes and phases of the signals. Subplot a) of Fig. 9 shows that the damping torque applied to the outer module (n =1) was approximately sinusoidal in shape. This suggests that the allowable damping torque was greater than the wave excitation torque. This resulted in the module velocities and powers being virtually 0, as shown in subplots b and c, respectively. Moving towards the centre modules, the damping torque

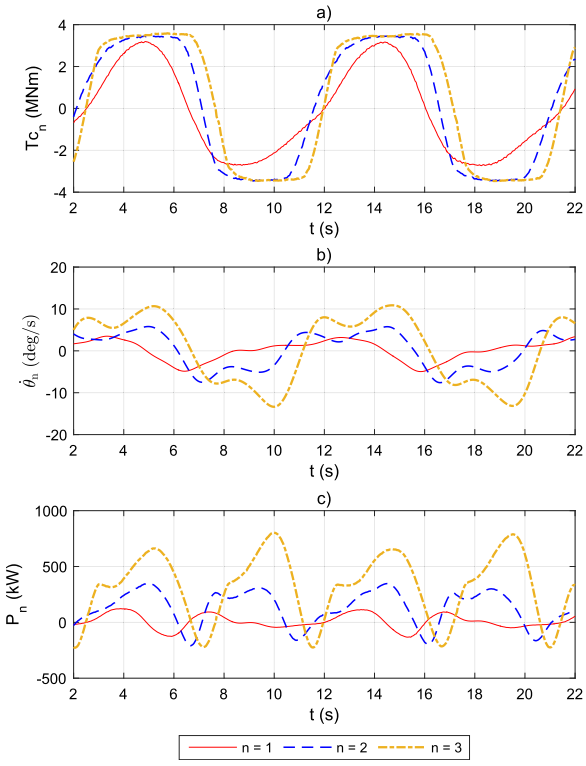

Fig. 9. Example of variation of individual module damping torques, Tc_n, (a), velocities, $\dot{\theta}_n$, (b) and powers, P_n, (c) for the nth modules, with time, t.

signals bared greater resemblance to Coulomb damping profiles. The magnitudes of the velocities and powers also increased.

The phase differences in the signals shown in Fig. 9 will have been caused by diffracted and radiated waves meeting the different modules at different points in time. The signals for symmetrical pairs, for example modules 3 and 4, were generally in phase. For adjacent modules on one half of the device though, phase differences were present. The greatest difference was between the outer and centre modules, for example numbers 1 and 3. From Fig. 9, differences of approximately 1/3 of the wave cycle were present in the velocity and power signals. Across the range of wave periods, there were phase differences in the velocities and powers, though no distinct relationship was shown. This means that the device was displaying similar behaviour to the out-of-phase motions shown by closely-spaced flap units in works such as Adamo and Mei (2005).

The instantaneous module power values were then averaged to find the mean module powers. Fig. 10 shows an example of results for the

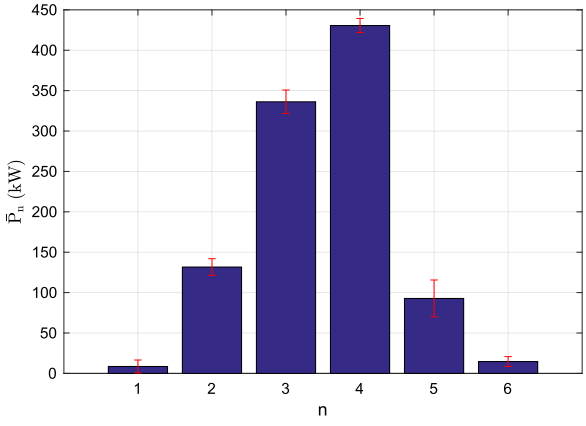

Fig. 10. Example of mean module powers, $\overline{P_n}$, for the nth modules, with combined expanded uncertainties shown as the error bars.

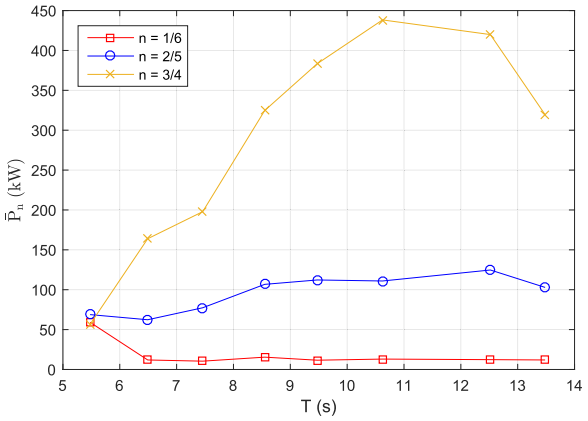

Fig. 11. Average mean powers per module for the nth symmetrical pairs of modules, $\overline{P_n}$, against wave period, T. The values are from tests that corresponded to the optimum recorded damping level.

same conditions as used for producing Fig. 9c). For this graph, though, the results for all modules are provided, to allow the reader to evaluate the level of symmetry present in the power measurements. Also shown are the uncertainties on the results.

Fig. 10 shows that there were some differences in the powers within modules paired around the centre of the device. The differences were due to a combination of tank effects, such as differences in amplitude across the wave crest, variations in module mass properties, imperfect damping control and sensor uncertainty. However, as also seen in Fig. 10, the absolute differences within the module pairs were far smaller than the differences between the pairs of results. This was generally true for the head-on waves. Hence, there was a reasonable level of symmetry in the results and so, for conciseness, the mean results for the pairs are subsequently used. The module pair mean power results are then compared in Fig. 11 across the range of wave periods.

Fig. 11 shows that the mean powers generally increased towards the centre of the device, with the outer most modules generating least power and the inner most modules generating most. This agrees with the findings by Sarkar et al. (2016). Averaging across the wave periods, the central modules (3/4) produced 68% of the total power, the inner modules (2/5) 25% and the outer modules (1/6) only 7%. It is likely that this was due to wave excitation torques increasing towards the centre, as shown in Sarkar et al. (2016).

As also indicated in Fig. 11, the variation of mean module powers changed with wave period. The 'coefficient of variation', a standard metric, was used for evaluating this. Variation was lowest, at 10%, for the shortest wave periods, and highest for the longer periods, maximising at 119% for a period of 10.6 s.

3.2. Modular Flap vs Rigid Flap

It is interesting to assess how the phase differences in the individual instantaneous module powers, shown in Fig. 9c, affected the total power produced by the Modular Flap. The same example as used in Fig. 9 was employed to explore this, in Fig. 12. Shown for comparison are also the equivalent results for the Rigid Flap.

Fig. 12 shows that the total power signal for the Modular Flap, when compared to the individual module powers in Fig. 9c, did not have the same relative magnitude of oscillations. While phase differences were shown in the module power values, the total power signal also combined into a single oscillation. However, it is also apparent that the variation in the Modular Flap power signal is lower than that associated with the Rigid Flap power. This was confirmed by calculation of the smoothness metric, S_P, as defined in Eq. (7), as 1.30 and 0.89 for the Modular and Rigid Flaps, respectively. To then gauge the general trend, a comparison of the smoothness metrics across the head-on wave conditions is provided in Fig. 13.

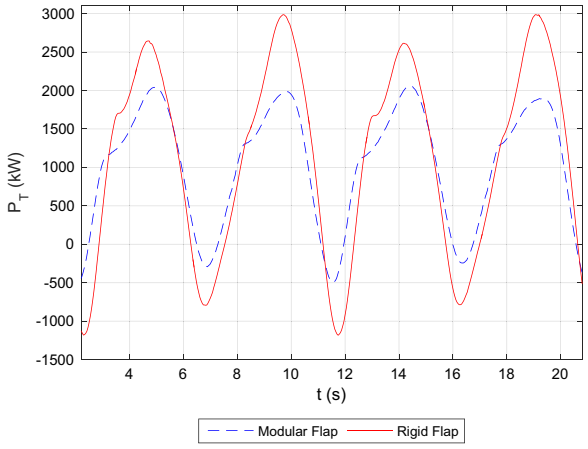

Fig. 12. Variation of total power, P_T, with time, t, for Modular and Rigid Flaps. Both devices had the same allowable total damping torque level applied to them. Note that the time has been adjusted so that the time-series approximately overlay.

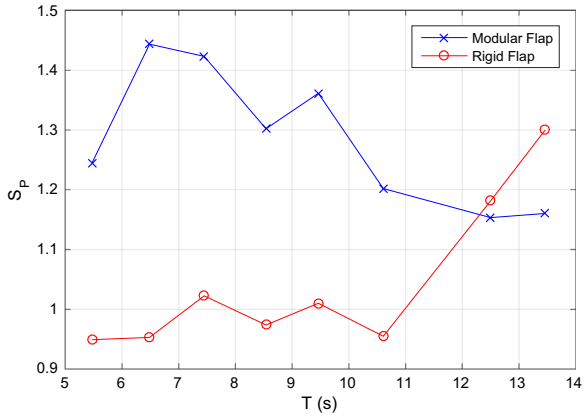

Fig. 13. Power smoothness metric, S_P, against wave period, T, for Modular and Rigid Flaps for head-on waves. Results are for damping level corresponding to maximum total mean power.

Fig. 13 shows that, for most of the wave periods, the smoothness metric was higher for the Modular Flap. On average, the total power produced by the Modular Flap was 23% more smooth. This was due to the out-of-phase power production by the individual modules, illustrated in Fig. 9c. This is an advantage for the Modular Flap as smoother, i.e. less variable, power production reduces cost requirements for energy storage for achieving electrical grid compliance (Molinas et al., 2007).

The capture factors, computed using Eq. (9), for the damping levels that resulted in maximum mean power capture were then computed. Presented first, in Fig. 14, are comparisons of the capture factors achieved by the two devices across the range of periods for the head-on waves.

Fig. 14 shows that both devices achieved relatively high capture factors across the range of wave periods, indicating a broad bandwidth. Though not well defined, both devices peaked at around a period of 10.6 s, with a capture factor of approximately 0.8. Fig. 14 also indicates that there was variation in the relative differences in the capture factors achieved by the two devices. Fig. 15 shows this in more detail by presenting the computed relative differences, using the Rigid Flap as the reference device, calculated with Eq. (10), for each wave period.

Fig. 15 shows that there was generally an inverse relationship between the relative differences in capture factor and the wave periods. For the lower wave periods, the Modular Flap outperformed the Rigid Flap, by up to 13%. This may have been due to a near-excitation of a natural mode of the system, such as shown for a similar device in Adamo and Mei (2005). For the higher periods though, the Rigid Flap

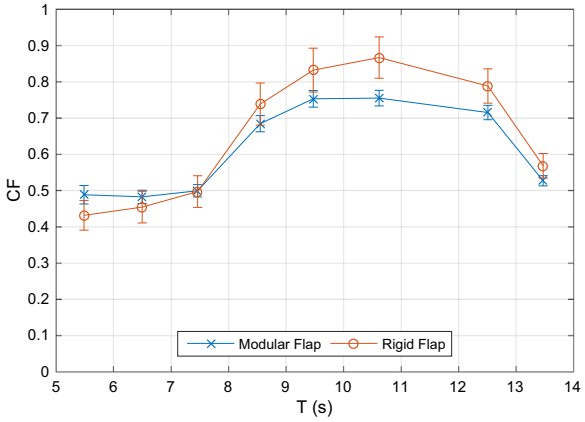

Fig. 14. Capture factors, *CF*, with associated expanded combined uncertainties, against wave period, T, for the Modular and Rigid Flaps in head-on waves.

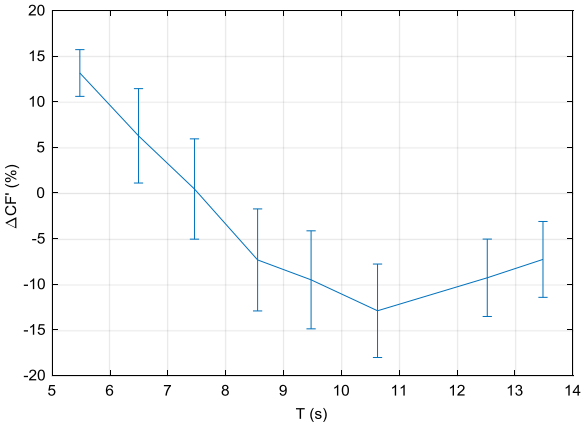

Fig. 15. Relative differences in the capture factors, *CF*, achieved by the two devices, using the Rigid Flap as the reference, ΔCF, with associated expanded combined uncertainties, against wave period, T, in head-on waves.

outperformed the Modular Flap, also by up to 13%. As one would imagine, the variation in the module power captures, shown in Fig. 11, was strongly correlated with the variation in the rotation amplitudes. Hence, there was an inverse correlation between the relative power production, shown in Fig. 15, and the level of variation in the module rotation amplitudes. This suggests that, with opening of larger gaps between the modules, greater water leakage occurred through the gaps, resulting in reduced power production. This suggests that higher power production is achieved by minimising the level of variation of the rotation of the modules. This could be realised by applying different damping levels to each module, as done in previous mathematical work (Sarkar et al., 2016). The effects of damping strategy on the power-capture of the Modular Flap is an area for further work.

The mean value of the relative differences in the capture factor across the wave periods, shown in Fig. 15, was then recorded. This was −3%, with an expanded combined uncertainty of +/- 5%. This shows that there was not a statistically significant reduction in efficiency when comparing the Modular Flap to the Rigid Flap.

For the head-on wave with an 8.5 s period, it was shown in Fig. 15 that the Modular Flap had 7% lower efficiency, with an uncertainty of +/- 6%. This shows that there was a statistically significant reduction in efficiency. This reduction may be offset by a superior performance in off-angle waves though. This hypothesis was tested by carrying out an equivalent evaluation on the off-angle results. First shown, in Fig. 16, are the capture factors achieved at different wave direction angles by the two devices.

Fig. 16 shows that the absolute deficit in the efficiency achieved by the Modular Flap compared to the Rigid Flap reduced as the wave

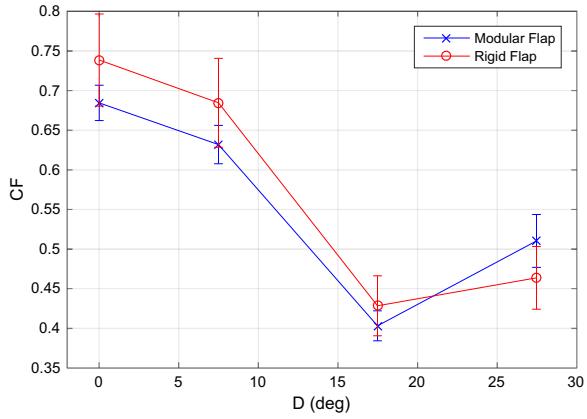

Fig. 16. Capture factors, *CF*, with associated expanded combined uncertainties, against wave direction, *D*, for the Modular and Rigid Flaps in off-angle waves.

direction angle grew. For both devices, the efficiency reduced due to a decrease in the net wave excitation torque acting on them. There is a difference though in the rate of this decrease and in the resistive torques applied by the devices. These differences, explored now, result in the distinctions between the rates of capture factor reduction with wave direction angle.

For rigid flaps that are narrow relative to the wavelength, the water particle motion that drives the flap can be approximated as being in phase across the flap width. The results of this is that the wave force acting on the flap simply decays with the cosine of the wave direction angle. The power capture is proportional to the wave force squared. Hence, for a narrow flap, the power capture reduces with the square of the cosine of the angle (Henry, 2008). The available power reduces with the cosine of the angle. Hence, the capture factor reduces with the cosine of the angle.

For flaps that are wider relative to the wave length though, the reduction is faster. This is because of two reasons. Firstly, the angle results in a phase difference in the wave torque across the flap. For the extreme case, the crest and trough of the flap would be at different ends of the flap, resulting in the wave torque being cancelled out (Henry, 2008). The hydrodynamic and body resistance to the wave torque, such as the added inertia, are independent of the wave angle. Hence, the reduced wave torque at any moment in time is having to overcome the same resistance. This results in reduced motions and hence power capture. The reduction in wave torque and hence power capture with wave angle is experienced by the Modular Flap too, but the rate is lower. This is because of the independence of the modules. Apart from at extreme wave angles, it is unlikely that there is any significant reduction in the wave torque due to the phase difference causing opposing forces across an individual module. Also, the increase of wave angle has the effect of reducing the body resistive forces for the Modular Flap. This is because the modules become decoupled and the wave torque must only overcome the added inertia, for example, of an individual module. The differences in the torques acting on the two devices are partly illustrated in the diagram provided in Fig. 17.

The combined effect of the two differences in the way that the devices respond to the changing wave direction is that the wave torque and power capture do not reduce as rapidly with the wave direction angle for the Modular Flap. As a result, it can be seen from Fig. 16 that the Modular Flap eventually outperforms the Rigid Flap. This comparison of the performances of the two devices is perhaps better illustrated in Fig. 18, which shows the relative differences in capture factors with wave direction angle.

Fig. 18 shows that the deficit in efficiency for the Modular Flap gradually reduces with increasing wave direction angle. At the largest angle of 27.5 degrees though, the Modular Flap performance was 10% greater. Although the quantity of results was limited, this shows that there was a point where the gains outweighed the losses for the Modular Flap. Hence, in a wave climate characterised by large directional variation, such as the Isle of Lewis in the Outer Hebrides (Wilkinson et al., 2014), a modular system could yield higher energy.

4. Conclusions

This paper has presented a power-capture assessment of a modular flap-type WEC, referred to here as the 'Modular Flap'. The device was made up of six modules, with a total width, at full-scale, of 33 m. Comparisons were made to a single equivalent unit, named the 'Rigid Flap'. The assessment was carried out with 30th scale physical modelling in a wave tank. The waves that were used were regular, with the period and direction varied and the amplitude held constant. The simplest damping strategy was employed, which was to damp each module equally. Results were generated both at module and device levels.

The power produced by the individual flap modules was very different, with power increasing significantly towards the centre. On average, the central pair of modules produced 68% of the total power, the inner modules 25% and the outer modules only 7%. This focusing of the power capture away from the outer modules was particularly prominent at longer wave periods. For sites characterised by these conditions, it may in fact therefore be most economical to have inexpensive structures, without PTOs, in place of the outer modules.

Phase differences were also shown between the powers produced by the modules. These caused a smoothing effect in the total instantaneous power. Using the inverse of the coefficient of variation as a metric, the Modular Flap produced power that was, on average, 23% more smooth. This could result in reductions in the costs associated with the energy storage that is needed for electrical grid compliance (Molinas et al., 2007).

For head-on waves, the average power-capture, measured using a capture factor, of the Modular Flap was 3% lower than the Rigid Flap. This difference had expanded combined uncertainty limits of +/− 5%. This shows that there was not a statistically significant reduction in power when using the Modular Flap. In previous literature (Sarkar et al., 2016), a range of damping strategies were applied. For the cases where equal damping coefficients were used on the flap modules, the total power capture was similar to that produced by the rigid flap used for comparison. The experimental work in this paper therefore provides some validation for this mathematical work. The paper also showed that superior power capture could be achieved by the modular system, even in head-on waves, by allowing the damping coefficients to vary across the modules (Sarkar et al., 2016). Hence, future complementary experimental work should focus on validating this case.

For off-angle waves, the Modular Flap experienced a lower rate of reduction in power-capture, with the wave direction angle, than the Rigid Flap. As a result, the deficit between the two devices reduced with increasing wave direction angle. Across the direction range, 7.5–27.5 degrees, the Modular Flap had average power capture that was 1% lower, with +/- 4% uncertainty, than that produced by the Rigid Flap. For the largest angle, though, the Modular Flap outperformed the Rigid Flap, by 10%, with +/- 1% uncertainty. This suggests that the Modular Flap would perform better in sites with large wave directional variation.

Combining the results for the head-on and off-angle wave conditions, it is likely that the average power captures across a range of sites would be similar for the Modular and Rigid Flaps. Along with previous literature (Sarkar et al., 2016), this work shows that it is unlikely that the adoption of the modular design would compromise the high conversion efficiency of the flap-type WEC (Babarit, 2015; Babarit et al., 2012). The Modular Flap has a number of techno-economic advantages, such as reduced parasitic foundation loads (Wilkinson et al., 2014), the possibility of less expensive installation, and, shown in this study, smoother power generation. These benefits can therefore be

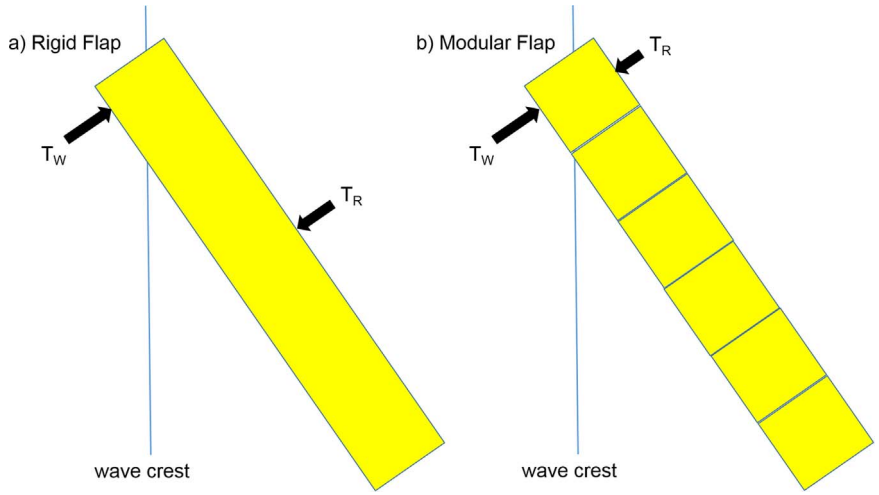

Fig. 17. Free body diagrams of torques acting on Rigid Flap (left) and Modular Flap (right) when met by an off-angle wave. T_W and T_R are the wave excitation and body resistance torques, respectively.

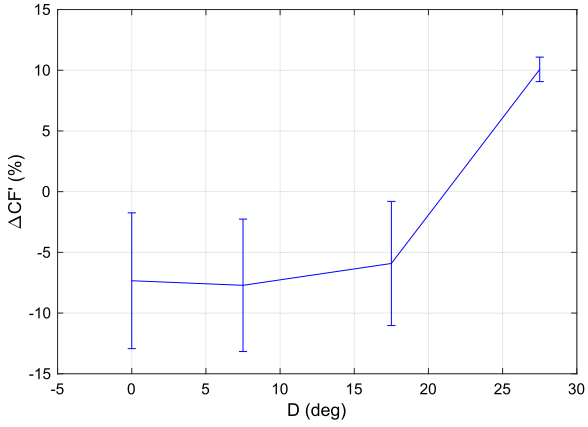

Fig. 18. Relative differences in the capture factors, *CF*, achieved by the two devices, using the Rigid Flap as the reference, Δ*CF*', with associated expanded combined uncertainties, against wave direction, D.

exploited without significantly compromising one of the flap-type WEC's greatest advantages, its efficiency.

Further work should evaluate the effects of the use of irregular and multi-directional waves. These, combined with resource occurrence tables, would allow for the estimation of annual energy productions. As discussed, the potential benefits of employing different damping control strategies should also be investigated. Optimisation of the modular concept, for example in terms of geometry, should also be carried out. This could investigate the effects of parameters such as the size of modules, the spacing between the modules and the total device width. Finally, an economic evaluation of the modular concept should be carried out, including estimated operational, maintenance and capital costs, to allow comparison to other energy sources (de Andres et al., 2016).

Acknowledgements

Thank you to the technicians at QUB, for design guidance and model fabrication, and to the QUB Marine Research Group, for support during the experimental campaign and writing of this paper. This work was supported by the Energy Technologies Institute (ETI) and the RCUK Energy Programme for the Industrial Doctoral Centre for Offshore Renewable Energy (grant number EP/J500847/1). Thank you also to the sponsors of this research, Aquamarine Power Ltd and QUB for financial support and the latter for provision of experimental testing facilities.

References

Abadie & Dias, 2016. Numerical Study of Wave Interaction with a Modular Oscillating Wave Surge Converter. In: Proceedings of the Twenty-Sixth (2016) International Ocean and Polar Engineering Conference.

Álvarez, 2015. Evaluation of Concepts to Reduce Structural Loading on The Wave Energy Converter Oyster. Technical University of Hamburg-Harburg.

de Andres, A., Maillet, J., Todalshaug, J.H., M??ller, P., Bould, D., Jeffrey, H., 2016. Techno-economic related metrics for a wave energy converters feasibility assessment. Sustain, 8. http://dx.doi.org/10.3390/su8111109.

Aquamarine Power Ltd, 2009. Oyster generates £1m for Orkney economy [WWW Document]. URL http://www.aquamarinepower.com/news/oyster-generates-£1m-for-orkney-economy.aspx (accessed 18.07.16).

Aquamarine Power Ltd, 2011. Projects: Oyster 800 project, Orkney [WWW Document]. URL ⟨http://www.aquamarinepower.com/projects/oyster-800-project-orkney.aspx⟩ (accessed 19.07.16).

AW-Energy, 2012. WaveRoller Concept [WWW Document]. URL ⟨http://aw-energy.com/about-waveroller/waveroller-concept⟩ (accessed 18.07.16).

Babarit, et al., 2012. Numerical benchmarking study of a selection of wave energy converters. Renew. Energy 41, 44–63. http://dx.doi.org/10.1016/j.renene.2011.10.002.

Babarit, 2015. A database of capture width ratio of wave energy converters. Renew. Energy 80, 610–628. http://dx.doi.org/10.1016/j.renene.2015.02.049.

Clabby, et al., 2012. The Effect of the Spectral Distribution of Wave Energy on the Performance of a Bottom Hinged Flap Type Wave Energy Converter. Rio de Janeiro.

Coleman, Steele, 2009. Experimentation, Validation, and Uncertainty Analysis for Engineers. John Wiley & Sons.

Folley, et al.2007. The design of small seabed-mounted bottom-hinged wave energy converters. In: Proceedings of the 7th European Wave and Tidal Energy Conference.

Henry, 2008. The Hydrodynamics of Small Seabed Mounted Bottom Hinged Wave Energy Converters in Shallow Water. Queen's University Belfast.

Henry, et al.2010. Advances in the Design of the Oyster Wave Energy Converter. In: Royal Institution of Naval Architect's Marine and Offshore Renewable Energy Conference. Royal Institution of Naval Architect's Marine and Offshore Renewable Energy Conference.

ITTC, 2014. ITTC – Recommended Procedures - General guideline for uncertainty analysis in resistance tests, (7.5-02-02-02)(Revision 02).

Lamont-Kane, et al.2013. In: vestigating Uncertainties in Physical Testing of Wave Energy Converter Arrays. In: Proceedings of the 10th European Wave and Tidal Energy Conference.

MathWorks, 2016. idealfilter [WWW Document]. URL ⟨http://uk.mathworks.com/help/matlab/ref/timeseries.idealfilter.html⟩ (accessed 09.03.16).

Mei, et al.1994. Subharmonic resonance of proposed storm gates for Venice Lagoon. In: Proceedings: Mathematical and Physical Sciences. doi:http://dx.doi.org/10.1098/rspa.1983.0054.

Molinas, et al.2007. Power Smoothing by Aggregation of Wave Energy Converters for Minimizing Electrical Energy Storage Requirements. In: Proceedings of the 7th European Wave and Tidal Energy Conference. doi:http://dx.doi.org/10.1016/j.tree.2005.11.022.

National Instruments, 2016. LabVIEW System Design Software [WWW Document]. URL ⟨http://www.ni.com/labview/⟩ (accessed 07.11.16).

O'Boyle, 2013. Wave Fields around Wave Energy Converter Arrays. Queen's University Belfast.

QUB, 2016. Portaferry Wave Tank [WWW Document]. URL ⟨http://www.qub.ac.uk/research-centres/cerc/Facilities/MarineFacilities/PortaferryWaveTank/⟩ (accessed 0708.16).

Renzi, et al., 2014. Wave-power absorption from a finite array of oscillating wave surge converters. Renew. Energy 63, 55–68. http://dx.doi.org/10.1016/

j.renene.2013.08.046.
Sammarco, et al., 2013. Flap gate farm: from Venice lagoon defense to resonating wave energy production. Part 1: natural modes. Appl. Ocean Res. 43, 206–213. http://dx.doi.org/10.1016/j.apor.2013.10.001.
Sarkar, et al., 2016. The modular concept of the Oscillating Wave Surge Converter. Renew. Energy 85, 484–497. http://dx.doi.org/10.1016/j.renene.2015.06.012.
United States Naval Academy, n.d. EN475 - Ocean Engineering Mechanics - Equation Sheet 1: Linear Wave Properties.
van 't Hoff, 2009. Hydrodynamic Modelling of the Oscillating Wave Surge Converter. Queen's Univ. Belfast.
Whittaker, Folley,, 2012. Nearshore oscillating wave surge converters and the development of Oyster. Philos. Trans. A. Math. Phys. Eng. Sci. 370, 345–364. http://dx.doi.org/10.1098/rsta.2011.0152.
Wilkinson, et al., 2014. Wave Loads on the Foundation of a Bottom-Hinged Modular Flap Structure. In: . Offshore Renewable Energy ORE.
Wilkinson, et al.2015. Modelling the performance of a modular flap-type wave energy converter. In: Proceedings of the 11th European Wave and Tidal Energy Conference.